Korean J. Chem. Eng., 34(12), 3111-3118 (2017)
DOI: 10.1007/s11814-017-0207-x

pISSN: 0256-1115
eISSN: 1975-7220

Compositional and structural variations of bitumen and its interactions with mineral matters during Huadian oil shale pyrolysis

Zhibing Chang, Mo Chu†, Chao Zhang, Shuxia Bai, Hao Lin, and Liangbo Ma

School of Chemical and Environmental Engineering, China University of Mining and Technology (Beijing), Beijing, China
(*Received 15 February 2017 • accepted 1 August 2017*)

Abstract−Thermal bitumen is an important intermediate derived from kerogen decomposition during oil shale pyrolysis. In this study, free bitumen (FB) and bound bitumen (BB) were obtained by extracting oil shale chars (300-550 °C) before and after demineralization, and then analyzed by liquid chromatography fractionation, Fourier transform infrared spectroscopy, and gas chromatography/mass spectrometry. The FB yield first increased and then decreased with increasing temperature, and the maximum value was 2.10% at 400 °C. The decarboxylation of acids and decomposition of esters at 350-450 °C decreased the content of these compounds. Meanwhile, the intense cracking reactions of aliphatic compounds and alkyl chains at 400-450 °C decreased the carbon chain lengths and molecular weights of these compounds. From the analytical results obtained for the BB fractions, we suggest that some carboxylic acids or carboxyl group-containing compounds may be trapped on carbonate particles by the formation of $Ca^{2+}COO^{-}$ bonds, whereas other oxygenated compounds (e.g., esters and phenols) can be adsorbed preferentially by clay minerals through Lewis acid-base interactions.

Keywords: Oil Shale Pyrolysis, Bitumen, Chemical Structure, Chemical Composition, Mineral Matters

INTRODUCTION

With the increasing global demand for oil and scarcity of appreciable oil reserves, oil shale, a fine-grained sedimentary rock that contains organic matter, is considered an important alternative source of crude oil. China has abundant oil shale resources that are estimated at approximately 720 billion tons (i.e., 47.6 billion tons of in-place shale oil) [1]. These huge energy reserves have great significance for alleviating pressure on petroleum supplies. Pyrolysis, or retorting, is one of the most attractive technologies applied in the utilization of oil shale. Kerogen, which is the main type of organic matter contained in oil shale, can be converted into shale oil by pyrolysis [2].

The term "Bitumen" is typically used to refer to the organic matter present in oil shale that is soluble in common organic solvents, such as benzene, chloroform, and methanol [3]. It is also defined as the organic solvent-soluble material produced by kerogen degradation and retained in spent shale during oil shale pyrolysis [4]. Taking bitumen as the intermediate material resulting from kerogen degradation, various decomposition schemes have proposed to model the kerogen degradation process [4-9]. One of the most frequently used models, which was proposed by Ziegel and Gorman [7], is shown in Fig. 1. This model divides the kerogen degradation process into two basic steps: first, kerogen is decomposed into solvent-soluble bitumen and some light oil and gas products; then, the organic matter within the bitumen is further cracked and/or vaporized into shale oil, gases, and coke with increasing temperature. The bitumen intermediate is not only the product of kerogen degradation but also the initial reactant that forms the final products. Thus, studying the formation characteristics and chemical structure features of this organic intermediate is highly important. Previous studies have primarily focused on the kinetics of bitumen formation and the conversion of bitumen to shale oil [4-8], the effects of kerogen type [10] and operation conditions [11-14] on bitumen formation, and the chemical structure transformation from kerogen to bitumen [15]. In contrast, few works have characterized the composition variation and chemical structure transformation of bitumen during its decomposition to oil, gas, and residue in detail, although this information is important to better understand the conversion pathway of bitumen and the formation mechanism of shale oil.

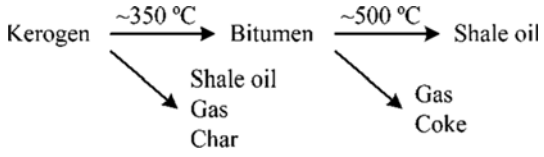

Fig. 1. Thermal pyrolysis process of kerogen [7].

Researchers [16-18] in the field of petroleum geochemistry have proposed the terms of "free bitumen" (FB) and "bound bitumen" (BB). FB is defined as the organic products generated from the thermal maturation of kerogen and readily extracted from the source rock, whereas BB refers to the organic products that are strongly adsorbed on the mineral matrix. Compared to FB, the extraction of BB requires the destruction of the mineral matrix. Comparing the compositions of FB and BB revealed that the mineral compo-

†To whom correspondence should be addressed.
E-mail: CCCUMTB@163.com
‡5th International Conference on Gasification and Its Application.

nents in sedimentary rocks retain the polar constituents of bitumen and, thus, affect petroleum generation and migration. Furthermore, argillaceous minerals are more active than other minerals such as carbonates and quartz [16]. Because substantial amounts of minerals are contained in oil shale, similar interactions between bitumen and minerals should occur during oil shale pyrolysis. Therefore, more direct evidence regarding the effects of minerals on kerogen pyrolysis should be provided by the compositions and structures of the BB fractions derived from oil shale pyrolysis.

We conducted pyrolysis experiments on Huadian oil shale at 300 °C, 350 °C, 400 °C, 450 °C, 500 °C, and 550 °C to obtain shale char samples. The shale char samples were subjected to sequential Soxhlet extraction-acid washing-Soxhlet extraction procedures to obtain FB, bitumen bound to carbonate, and bitumen bound to silicate. Liquid column chromatography, Fourier transform infrared (FTIR) spectroscopy, and gas chromatography/mass spectrometry (GC/MS) were used to analyze the chemical compositions and structural features of these bitumen fractions. The purpose of this study was to characterize the composition variation and structure transformation of bitumen during oil shale pyrolysis. The interactions between bitumen and mineral matters were also explored by comparing the analytical results obtained from the FB and BB fractions.

MATERIALS AND METHODS

1. Materials

The oil shale sample was obtained from Huadian, Jilin province, China. Table 1 shows the chemical properties of the sample. The proximate analysis was conducted according to GB/T 212-2008. The C, H, N, and S contents were determined with a vario MACRO cube CHNS elemental analyzer, and the O content was calculated by difference. The original oil shale was crushed, ground, and sieved to a grain size smaller than 0.2 mm. All samples were dried in a 110 °C oven for 5 h and then stored in a desiccator for subsequent experiments.

2. Pyrolysis of Oil Shale

Pyrolysis experiments of oil shale were conducted in a fixed-bed reactor, as schematically illustrated in Fig. 2. The reactor was made of stainless steel, and a stainless steel pipe was welded to the cover of the reactor for carrier gas inlet. Approximately 50 g of raw oil shale was placed inside the reactor, which was installed in an electric-ring furnace with a thermocouple inserted. Then, it was heated from ambient temperature to 300 °C, 350 °C, 400 °C, 450 °C, 500 °C, and 550 °C at a heating rate of 5 °C/min and held at the final temperature for 30 min. Nitrogen gas was introduced into the reactor at a flow rate of 50 mL/min to sweep the volatile products out of the reactor. The evolved oil vapor, water steam, and gases were

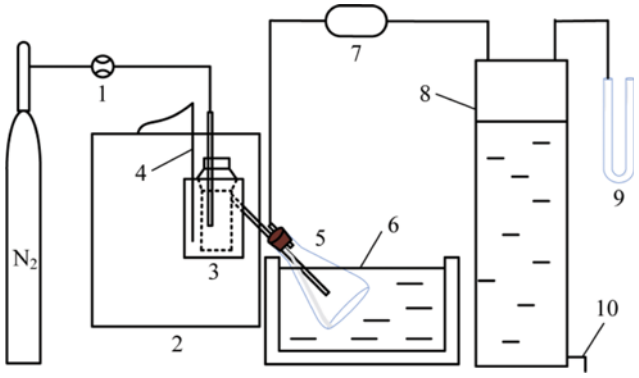

Fig. 2. Schematic diagram of the fixed bed pyrolysis reactor system.

1. Mass flow controller
2. Electric-ring furnace
3. Stainless steel reactor
4. Thermocouple
5. Conical flask
6. Ice-water bath
7. Drying tube
8. Plexiglas cylinder
9. U-tube manometer
10. Water faucet

channeled into a conical flask that was immersed in an ice-water bath. Most of the water and oil condensed in the flask, and the residual portion was captured by a drying tube filled with cotton wool and silica gel. The non-condensable gases were collected in a Plexiglas cylinder by the water displacement method.

After the conclusion of each run, the apparatus was disassembled. The mass of shale char was weighed directly, and the mass of the mixture of shale oil and water was determined from the mass difference between the collecting flask before and after pyrolysis. The water in the oil/water mixture was determined by the Dean-Stark method using toluene as a solvent. The mass of shale oil was obtained by the mass difference, and the shale oil yield was calculated according to Eq. (1):

$$\text{Shale oil yield (\%)} = \frac{\text{Mass of shale oil (g)}}{\text{Mass of oil shale (g)}} \times 100 \quad (1)$$

3. Thermal Bitumen Extraction

Thermal bitumen was separated from the shale char in a Soxhlet apparatus according to the scheme presented in Fig. 3. Chloroform was used as the solvent because of the good solubility of Huadian oil shale thermal bitumen in this solvent [15]. A 24-h Soxhlet extraction was performed on the shale char to recover FB. Following the first extraction, the remaining non-extractable material was demineralized using 6 mol/L hydrochloric acid (HCl) at 60 °C for 8 h, and the solid residue was washed, filtered, and dried. A second 24-h Soxhlet extraction was performed on the remaining material to recover BB-1. Subsequently, the remaining non-extractable material was demineralized again utilizing 40 wt% hydrofluoric acid (HF) at 60 °C for 8 h, and the residual organic matter was

Table 1. Proximate and ultimate analyses of Huadian oil shale

Proximate analysis (air dried basis) (wt%)				Ultimate analysis (air dried basis) (wt%)				
H_2O	Volatiles	Ash	Fixed carbon	C	H	N	S	O[a]
5.42	23.30	69.23	2.05	15.75	1.97	0.47	1.16	6.76

[a]By difference

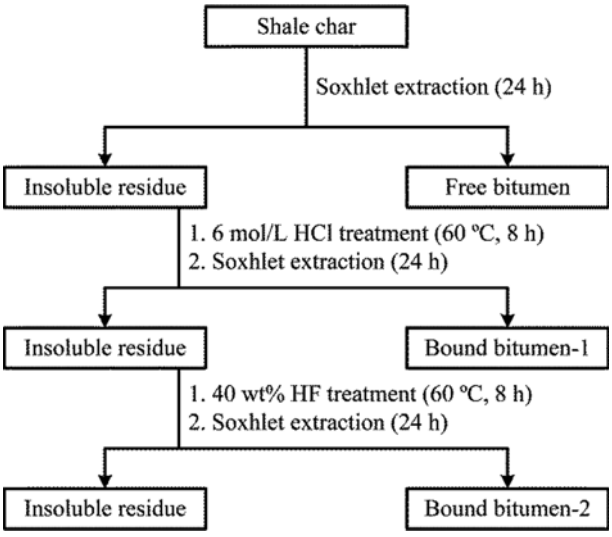

Fig. 3. Schematic diagram of the bitumen extraction procedure.

washed, filtered, and dried. A third 24-h Soxhlet extraction of the remaining organic matter was performed to recover BB-2. The chloroform was evaporated from the bitumen solutions at approximately 40 °C and slightly reduced pressure to recover the bitumen samples, which were then weighed to calculate the bitumen yield and reserved for subsequent analyses. The bitumen yield was calculated with Eq. (2):

$$\text{Bitumen yield (\%)} = \frac{\text{Mass of bitumen (g)}}{\text{Mass of oil shale (g)}} \times 100 \quad (2)$$

X-ray diffraction (XRD) analyses of raw oil shale, shale char, and their demineralization products were performed on a Rigaku D/max-2500PC diffractometer with Cu Kα radiation (λ=1.5418 Å). The tube voltage and tube current were 40 kV and 100 mA, respectively. Diffraction patterns were taken from 2.5° to 70° at 4°/min in 0.02° increments. The minerals present in oil shale samples were identified by comparing the X-ray spectra with a database.

4. Analyses of Bitumen Fractions

The chemical class compositions of the bitumen fractions were determined according to SY/T 5119-2008. Briefly, approximately 30 mL of hexane was added to 30-50 mg of bitumen sample. Then, the mixture was allowed to sit for 12 h and filtered through a funnel covered with cotton wool. The hexane-insoluble matter remaining on the cotton wool was washed with hexane until the filtrate was clear. Next, the hexane-insoluble asphaltenes retained on the cotton wool were rinsed with chloroform until the washing liquid was colorless. Thus, the asphaltene solution was obtained. The solution containing the hexane-soluble matter was concentrated to 3-5 mL. A mini glass column (7 mm×400 mm) was packed with 3 g of silica gel and 2 g of neutral alumina. After the hexane solution was poured through the packed column, 25 mL of hexane was added to elute the saturate fraction. Subsequently, a 20-mL mixture of hexane/dichloromethane (1 : 2, v/v) was used to obtain the aromatic fraction. The resin fraction was obtained by eluting the column with 10 mL of ethanol, followed by 15 mL of chloroform. Finally, the obtained saturate, aromatic, resin, and asphaltene (SARA) solutions were evaporated in a rotary evaporator to recover the corresponding fractions, which were weighed to calculate the chemical class compositions of the bitumen samples.

FTIR analysis was conducted on a Nicolet 6700 spectrometer to characterize the structural changes of bitumen during pyrolysis. The FTIR experiments were conducted at a resolution of 4 cm^{-1} over a wave number range of 4,000-400 cm^{-1}.

The detailed composition of the bitumen samples was determined by GC/MS analysis conducted on a Thermo SCIENTIFIC GC equipped with a Trace 1300-ISQ MS. The chemical compounds were identified using the National Institute of Standards and Technology mass spectral library.

RESULTS AND DISCUSSION

1. XRD Characterization of Raw Oil Shale and Shale Char Samples

The XRD analyses of raw oil shale and shale char samples are shown in Fig. 4(a). The dominant mineral phases identified in the raw oil shale were quartz, calcite, montmorillonite, illinite, kaolite, and pyrite. The momtmorillonite peak shifted from 2θ=7.3° to 2θ=8.9° after pyrolysis at 300 °C because of the removal of water

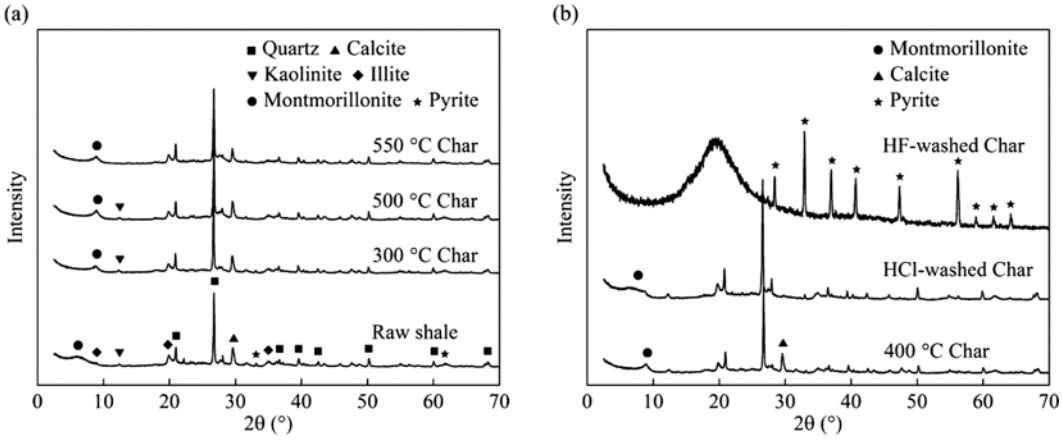

Fig. 4. XRD patterns of shale chars (a) and the demineralization products of 400 °C char (b).

associated with exchangeable cations. The reduction in the interlayer space increased the diffraction angle of montmorillonite. The obtained spectra do not show obvious variation at 300-500 °C. However, the diffraction peak of kaolinite at 2θ=12.3° disappears at 550 °C because of the dehydroxylation reactions of kaolinite [19].

Fig. 4(b) presents the XRD spectra of 400 °C char and its demineralization products. The peak at 2θ=29.5°, which is attributed to calcite, is absent in the spectrum of HCl-washed char because calcite was removed by the HCl treatment. After washing with HF, the characteristic peaks of quartz and clay minerals disappeared, indicating that the silicates were eliminated. Because the majority of the mineral matrix was removed, pyrite was concentrated selectively, and its peaks became more intense. Additionally, the broad hump at approximately 2θ=20° was mainly ascribed to n-alkanes and naphthenes [20,21]. The XRD analyses of other shale char samples and their demineralization products produced results similar to those obtained for the 400 °C char. As shown in Fig. 3, BB-1 was obtained by extracting shale char after HCl washing, and BB-2 was obtained by extracting shale char after further HF washing. Therefore, BB-1 and BB-2 can be considered as organic products that are strongly absorbed on carbonates and silicates, respectively.

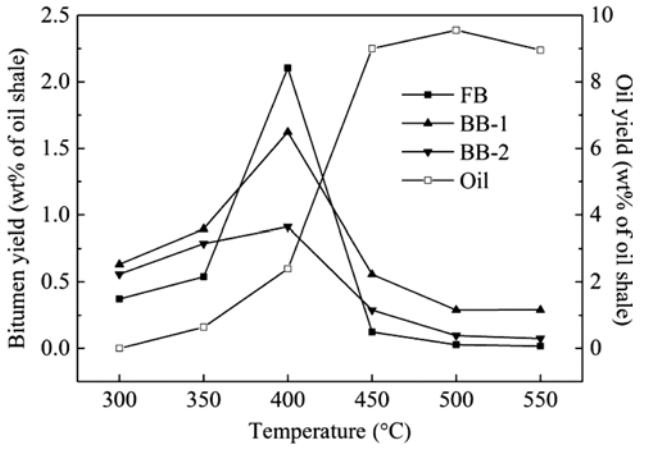

Fig. 5. The effect of the pyrolysis temperature on the yields of bitumen and shale oil.

2. Bitumen Yield

Fig. 5 shows the bitumen and shale oil yields as a function of temperature. All data are plotted as percentages of the raw oil shale to facilitate comparison. No shale oil was produced at 300 °C, whereas the FB, BB-1, and BB-2 yields were 0.37%, 0.63%, and 0.56%, respectively. Thus, the kerogen was likely not decomposed, and a significant part of the bitumen appears to be the inherent bitumen in oil shale. The FB, BB-1, and BB-2 yields increased with increasing temperature from 300 °C to 400 °C and reached their maximal values of 2.10%, 1.62%, and 0.91%, respectively, at 400 °C. In comparison, during the pyrolysis of Longkou oil shale pyrolysis, the FB yield peaked at approximately 440 °C [22]. This discrepancy may be attributed to the chemical structure of kerogen because Longkou kerogen is a type II kerogen [23]. As the pyrolysis temperature increased from 400 °C to 550 °C, the FB, BB-1, and BB-2 yields decreased to 0.02%, 0.29%, and 0.07%, respectively. In particular, the drop gradient between 400 °C and 450 °C was significantly sharper than those in other zones. This is because most bitumen cracks or vaporizes into shale oil at 400-450 °C [24]. Indeed, the shale oil yield increases obviously from 2.39% at 400 °C to 9.00% at 450 °C. Fig. 5 also shows that the BB-1 yield was higher than the BB-2 yield throughout the temperature range tested, indicating that during pyrolysis, the absorption capacity of carbonates is larger than that of silicates.

3. Bitumen Characterization

Chemical class fractionation, FTIR, and GC/MS were employed to analyze the chemical compositions and structures of different bitumen fractions. As the bitumen yields changed dramatically over 350-450 °C, the bitumen fractions obtained at 350 °C, 400 °C, and 450 °C were selected for analysis.

3-1. Chemical Class Fractionation

Fig. 6 shows the weight percentages of SARA fractions in bitumen samples extracted from char samples obtained at 350 °C, 400 °C, and 450 °C. Fig. 6(a) indicates that FB samples are characterized by relatively high resin contents that account for approximately half of the FB samples. The chemical class composition of FB remained almost constant as the temperature was increased

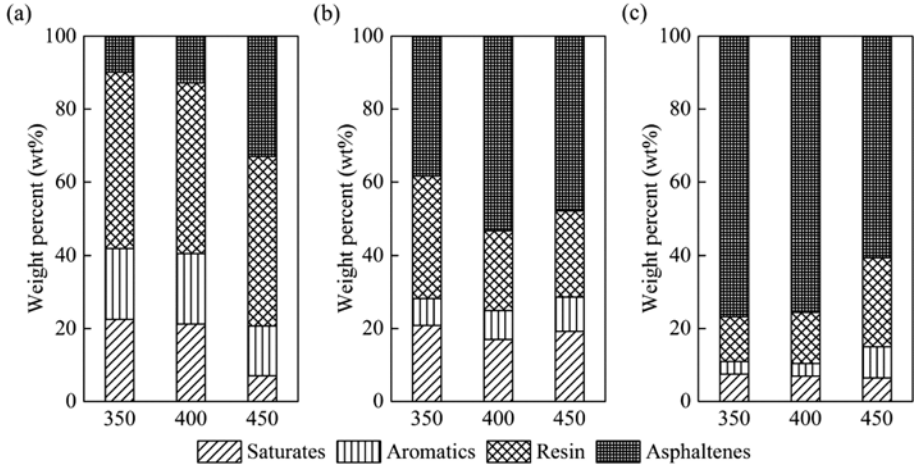

Fig. 6. Chemical class compositions of FB (a), BB-1 (b), and BB-2 (c) resulting from oil shale pyrolysis.

from 350 °C to 400 °C, indicating that kerogen degradation produces an organic intermediate with a relatively constant composition. However, as the temperature was further increased from 400 °C to 450 °C, the contents of saturates and aromatics decreased obviously, whereas the asphaltene content increased from 12.78% to 33.01%. The reduction in saturates and aromatics is mainly the result of the cracking and vaporization of these compounds at higher temperatures. When aliphatic hydrocarbons and aromatic hydrocarbons were cracked or vaporized to form shale oil, the asphaltene fraction was concentrated selectively in the FB. Additionally, the kerogen degradation proceeded more completely at higher temperatures, producing additional asphaltenes and, thus, increasing the content of this fraction [25].

The BB-1 and BB-2 samples were composed of organic products absorbed on carbonates and silicates, respectively. Compared with the FB samples, the BB-1 samples generally had smaller saturates, aromatics, and resin fractions and larger asphaltene fractions (Fig. 6(b)), indicating that carbonates absorb polar components preferentially. Jovančićević et al. [17] also reported that carbonates can absorb resins and asphaltenes. This absorption ability may be related to the formation of alkaline M^{2+}-O groups via interactions of the alkaline earth metal cations in the carbonates with -COOH and -OH groups [26]. Fig. 6(c) shows that asphaltene compounds constituted the main component of BB-2 (i.e., 60-77% of BB-2), suggesting that silicates can combine with highly polar compounds with high molecular weights. Huizinga et al. [16] noted that some polar constituents produced from kerogen pyrolysis may become adsorbed on illite and montmorillonite via the formation of strong organic-mineral chemical bonds. Siskin et al. [27,28] also found that acid-base interactions between organics and clay minerals bind kerogen to the mineral matter of oil shale. The chemical composition of BB varies with temperature. Notably, as the temperature increased from 400 °C to 450 °C, the content of saturates in BB-1 increased slightly. This phenomenon may be attributable to the depolymerization and cracking of macromolecular compounds (i.e., resins and asphaltenes) becoming more active at 450 °C, and producing many aliphatic hydrocarbons. Some of the aliphatic hydrocarbons were confined in the mineral matrix of the oil shale. As the carbonate minerals were removed by HCl washing, they were released and incorporated into BB-1 during $CHCl_3$ extraction.

3-2. FTIR Analysis

Fig. 7 presents the FTIR spectra of bitumen fractions derived by pyrolyzing oil shale at 350 °C, 400 °C, and 450 °C. According to the reported FTIR absorption bands of bitumen [15,29] and kerogen

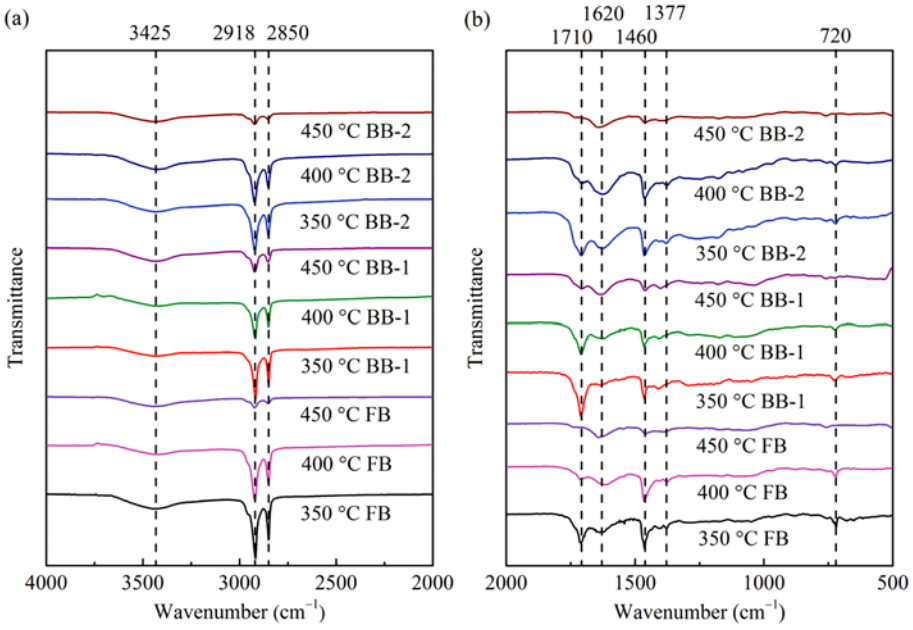

Fig. 7. FTIR spectra of bitumen samples in the ranges of 4,000-2,000 cm^{-1} (a) and 2,000-500 cm^{-1} (b).

Table 2. A summary of the FTIR characteristic bands of some functional groups in bitumen samples

Peak (cm^{-1})	Band assignments
3425	-OH stretching of phenols and carboxylic acids
2918, 2850	Asymmetrical and symmetrical stretching of alkyl CH_2 groups
1710	C=O stretching of carboxyl or carbonyl groups
1620	C=C stretching of aromatic rings
1460	Asymmetric bending of CH_3 and CH_2 groups
1377	Symmetric bending of CH_3 groups
720	Skeletal vibration of straight chains containing more than four CH_2 groups

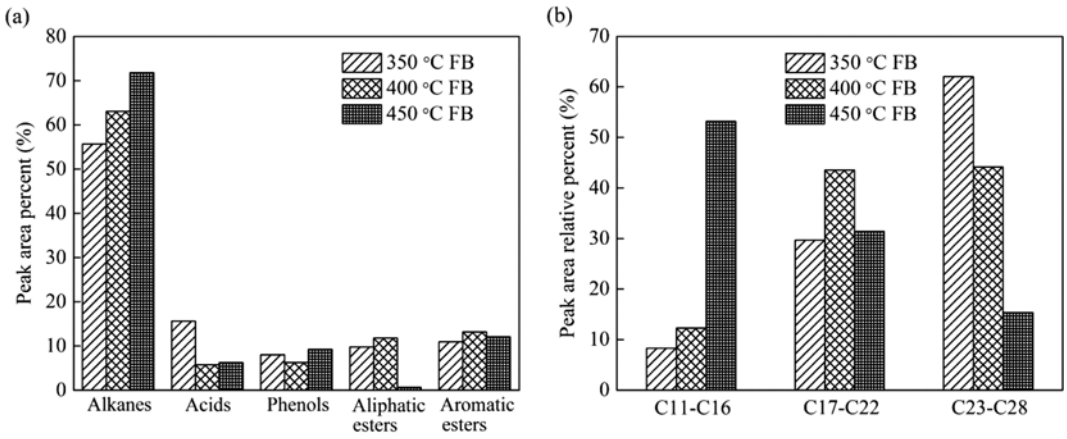

Fig. 8. Peak area percent values of major species (a) and carbon number distribution of *n*-alkanes (b) in FB samples.

[22,30], a summary of the FTIR characteristic bands of some functional groups in bitumen samples is shown in Table 2.

In the spectra of FB samples, as the temperature was increased from 350 °C to 400 °C, the intensity of the band at 1,710 cm^{-1} decreased, indicating that a considerable amount of C=O groups was decomposed at 400 °C. Additionally, the intensity of the band at 1,620 cm^{-1} increased slightly because more aromatic compounds were derived from kerogen degradation at 400 °C. Further increasing the temperature from 400 °C to 450 °C resulted in an obvious decrease in the intensity of the bands at 2,918 cm^{-1}, 2,850 cm^{-1}, 1,460 cm^{-1}, 1,377 cm^{-1}, and 720 cm^{-1}. Thus, the cracking and vaporization of alkanes became more active, which reduced the amount of aliphatic carbons and decreased the chain length of alkanes. Furthermore, the band at 1,710 cm^{-1} almost disappeared, indicating the nearly complete decomposition of C=O groups or vaporization of these oxygenated compounds at 450 °C.

Compared with the FB fraction, the BB-1 fraction typically exhibited a more intense band at 1,710 cm^{-1}; thus, BB-1 contains more C=O groups than FB. These abundant C=O groups may be related to the formation of M^{2+}-O groups, which could act as a binding material linking the organic products to carbonate minerals. BB-2 samples had more intense bands at 1,620 cm^{-1} than BB-1 samples, implying that BB-2 samples are more aromatic in nature. This finding is consistent with the chemical class composition results. For both BB-1 and BB-2, the intensity of the bands attributed to aliphatic carbons (2,918 cm^{-1}, 2,850 cm^{-1}, 1,460 cm^{-1}, 1,377 cm^{-1}, and 720 cm^{-1}) decreased to varying extents between 400 °C and 450 °C because of the cracking and vaporization of aliphatic compounds and the cleavage of the lateral alkyl chains of aromatic compounds [24].

3-3. GC/MS Analysis

GC/MS was applied to further investigate the detailed compositions of the bitumen samples [31-33]. Note that GC/MS can only detect light compounds with boiling points below 300 °C. Fig. 8(a) presents the area percentages of the major components detected in FB samples. When the pyrolysis temperature was varied from 350 °C to 400 °C, the carboxyl acid content decreased from 15.57% to 5.77%, the alkane content increased from 55.67% to 63.03%, and the content of other components remained relatively constant. Thus, decarboxylation occurred and converted acids into alkanes between 350 °C and 400 °C. As the temperature increased from 400 °C to 450 °C, the aliphatic ester content decreased from 11.77% to 0.63%, whereas the content of alkanes increased from 63.03% to 71.78%. These findings indicate that the decomposition of ester groups is intense at 400-450 °C. These results are consistent with the preceding observation that the amount of C=O groups decreased at 350-450 °C. *n*-Alkanes in FB were divided into groups of C11-C16, C17-C22, and C23-C28 according to the carbon number, as shown in Fig. 8(b). Clearly, raising the temperature gradually decreased the alkane fraction with long carbon chains, but increased the alkane fraction containing short carbon chains. This is because the cracking reactions of alkanes were more active at high temperatures. The active cracking and vaporization of alkanes were also confirmed by Fig. 7, which shows that some aliphatic carbon bands exhibited decreased intensity or disappeared in the FTIR spectra of FB from 350 °C to 450 °C.

Fig. 9 compares the compositions of FB, BB-1, and BB-2 produced at 400 °C. Clearly, carboxylic acids comprised approximately 70% of BB-1 and were, thus, the main detectable compounds. This

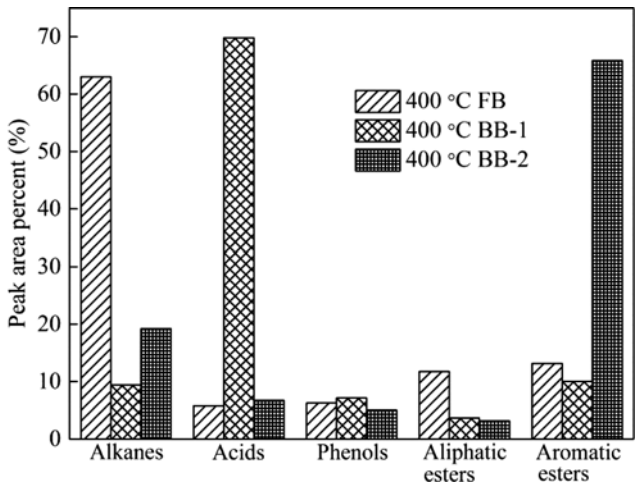

Fig. 9. Peak area percentages of major components in bitumen samples obtained at 400 °C.

finding confirms the reaction of carboxylic acids and inherent carbonates. Huizinga et al. [16] and Hu et al. [34] indicated that the organic acids resulting from kerogen degradation should react with carbonates to generate carboxylates and carbon dioxide. Fig. 9 also shows that oxygenated compounds, including acids, phenols, and esters, account for more than 80% of the detectable compounds in BB-2, which consists of organic products absorbed on silicates. The adsorption of oxygenated compounds on silicates may be attributed to the presence of clay minerals. Previous studies [16,17] have demonstrated that clay minerals can adsorb polar heteroatomic compounds and that montmorillonite has the most pronounced adsorptive effects.

4. Interactions between Bitumen and Mineral Matters

The results of both FTIR and GC/MS indicated that the carboxylic acids and carboxyl group-containing compounds resulting from kerogen decomposition can react with inherent carbonates to form carboxylates as described by Eqs. (3) and (4). The $Ca^{2+}COO^{-}$ bonds formed are thought to link the organic products to carbonate minerals. The clay minerals present in Huadian oil shale, including montmorillonite, illite, and kaolinite, are layered aluminosilicates. During oil shale pyrolysis, the exchangeable cations in the interlayers of montmorillonite may be dehydrated to form Lewis acid sites. Additional Lewis acid sites are contributed by Al^{3+} and Fe^{3+} in octahedral coordination exposed at the broken-edge bonds of crystallites. These Lewis acid sites enable clay minerals to act as electron-pair acceptors during pyrolysis. In contrast, the esters, phenols, and acids derived from kerogen pyrolysis can act as electron-pair donors because they have lone pair electrons on their oxygen atoms. Consequently, oxygenated compounds can combine with clay minerals through acid-base interactions, as shown by Eq. (5).

$$\text{Bit-COOH}+\text{CaCO}_3 \rightarrow \text{Ca(HCO}_3\text{)(Bit-COO)} \quad (3)$$

$$\text{Bit}'\text{-COOH}+\text{Ca(HCO}_3\text{)(Bit-COO)} \rightarrow \text{Ca(Bit-COO)(Bit}'\text{-COO)}+\text{H}_2\text{O}+\text{CO}_2 \quad (4)$$

$$\text{Bit-O}:+\text{Clay-M}^{m+} \rightarrow \text{Bit-O}:\text{M}^{m+}\text{-Clay} \quad (5)$$

CONCLUSIONS

The compositional variation and chemical structure transformation of bitumen during Huadian oil shale pyrolysis were studied. The decarboxylation of acids and decomposition of esters at 350-450 °C decreased the acid and ester contents in FB. Meanwhile, the intense cracking of aliphatic carbon chains at 400-450 °C decreased the aliphatic carbon content and shortened the carbon chain length.

The interactions between bitumen and mineral matters were explored by characterizing the composition and structure of BB. During oil shale pyrolysis, some carboxylic acids or carboxyl group-containing compounds can be trapped on carbonate particles by the formation of $Ca^{2+}COO^{-}$ bonds, whereas other oxygen-containing compounds, such as esters and phenols, can be adsorbed preferentially by clay minerals through Lewis acid-base interactions.

The bitumen yields first increased and then decreased as the temperature increased from 300 °C to 550 °C and reached their maximal values at 400 °C. Most of the bitumen cracked or vaporized into shale oil between 400 °C and 450 °C, significantly decreasing the yields of FB, BB-1, and BB-2 from 2.10%, 1.62%, and 0.91% to 0.12%, 0.57%, and 0.29%, respectively.

ACKNOWLEDGEMENTS

This study was financially supported by the National Basic Research Program of China (Grant No. 2014CB744301). As this study was presented at 5th International Symposium on Gasification and Its Application (iSGA-5), the authors greatly appreciate the committee of iSGA-5.

REFERENCES

1. Z. J. Liu, Q. S. Dong, S. Q. Ye, J. W. Zhu, W. Guo, D. C. Li, R. Liu, H. L. Zhang and J. F. Du, *J. Jilin. Univ.*, **36**, 869 (2006).
2. A. K. Burnham and J. A. Happe, *Fuel*, **63**, 1353 (1984).
3. M. S. Solum, C. L. Mayne, A. M. Orende and R. J. Pugmire, *Energy Fuel*, **28**, 453 (2014).
4. A. K. Burnham, in *Oil Shale: A Solution to the Liquid Fuel Dilemma*, O. I. Ogunsola, A. M. Hartstein and O. Ogunsola Eds., ACS Symposium Series 1032, Washington DC (2010).
5. A. B. Hubbard and W. E. Robinson, *USBM Rep. Invest.?U.S. Bur. Mines*, 4744 (1950).
6. R. L. Braun and A. J. Rothman, *Fuel*, **54**, 129 (1975).
7. E. R. Ziegel and J. W. Gorman, *Technometrics*, **22**, 139 (1980).
8. P. H. Wallman, P. W. Tamm and B. G. Spars, in *Oil Shale, Tar Sands and Related Materials*, H. Stauffer Eds., ACS Symposium Series 163, Washington DC (1981).
9. C. S. Wen and T. P. Kobylinski, *Fuel*, **62**, 1269 (1983).
10. F. P. Miknis, T. F. Turner, G. L. Berdan and P. J. Conn, *Energy Fuel*, **1**, 477 (1987).
11. L. Tiikma, A. Zaidentsal and M. Tensorer, *Oil Shale*, **24**, 535 (2007).
12. J. Sokolova, L. Tiikma, M. Bityukov and I. Johannes, *Oil Shale*, **28**, 4 (2011).
13. Y. Fei, M. Marshall, W. Roy Jackson, M. L. Gorbaty, M. W. Amer, P. J. Cassidy and A. L. Chaffee, *Fuel*, **92**, 281 (2012).
14. P. W. Zhao, Y. J. Zhao, C. J. Zou and T. Gu, *Oil Shale*, **30**, 491 (2013).
15. Q. Y. Li, X. X. Han, Q. Q. Liu and X. M. Jiang, *Fuel*, **121**, 109 (2014).
16. B. J. Huizinga, E. Tannenbaum and I. R. Kaplan, *Org. Geochem.*, **11**, 591 (1987).
17. B. Jovančićević, D. Vitorović, M. Šaban and H. Wehner, *Org. Geochem.*, **18**, 511 (1992).
18. M. Razvigorova, T. Budinova, B. Tsyntsarski, B. Petrova, E. Ekinci and H. Atakul, *Int. J. Coal. Geol.*, **76**, 243 (2008).
19. J. H. Patterson, *Fuel*, **73**, 321 (1994).
20. J. W. Yan, X. M. Jiang, X. X. Han and J. G. Liu, *Fuel*, **104**, 307 (2013).
21. Y. S. Yin, J. Zhang and C. D. Sheng, *Korean J. Chem. Eng.*, **26**, 895 (2009).
22. W. Wang, Y. Ma, S. Y. Li, J. Shi and J. S. Teng, *Energy Fuel*, **30**, 830 (2016).
23. Q. Wang, Z. Y. Huang, M. S. Chi, J. X. Shi, Z. C. Wang and Y. Sui, *CIESC J.*, **66**, 1861 (2015).
24. S. Wang, X. M. Jiang, X. X. Han and J. H. Tong, *Fuel Process. Technol.*, **121**, 9 (2014).

25. A. K. Burnham, in *Oil Shale, Tar Sands and Related Materials*, H. Stauffer Eds., ACS Symposium Series 163, Washington DC (1981).
26. A. Karabakan and Y. Yürüm, *Fuel*, **77**, 1303 (1998).
27. M. Siskin, G. Brons and J. F. Payack, *Energy Fuel*, **1**, 248 (1987).
28. M. Siskin, G. Brons and J. F. Payack, *Energy Fuel*, **3**, 108 (1989).
29. S. Yoon, S. D. Bhatt, W. Lee, H. Y. Lee, S. Y. Jeong, J.-O. Baeg and C. W. Lee, *Korean J. Chem. Eng.*, **26**, 64 (2009).
30. J. H. Tong, X. X. Han, S. Wang and X. M. Jiang, *Energy Fuel*, **25**, 4006 (2011).
31. H. Sutcu, *Korean J. Chem. Eng.*, **24**, 736 (2007).
32. P. Weerachanchai, C. Tangsathitkulchai and M. Tangsathitkulchai, *Korean J. Chem. Eng.*, **28**, 2262 (2011).
33. Y.-M. Kim, T. U. Han, B. Hwang, B. Lee, H. W. Lee, Y.-K. Park and S. Kim, *Korean J. Chem. Eng.*, **33**, 2350 (2016).
34. M. J. Hu, Z. Q. Cheng, M. Y. Zhang, M. Z. Liu, L. H. Song, Y. Q. Zhang and J. F. Li, *Energy Fuel*, **28**, 1860 (2014).